Materials Chemistry and Physics 145 (2014) 278–287

Contents lists available at ScienceDirect

Materials Chemistry and Physics

journal homepage: www.elsevier.com/locate/matchemphys

Terahertz time-domain spectroscopy response of amines and amino acids intercalated smectites in far-infrared region

M. Janek [a,*], D. Zich [a], M. Naftaly [b]

[a] Comenius University, Faculty of Natural Sciences, Department of Physical and Theoretical Chemistry, Mlynská dolina CH1, SK-84215 Bratislava, Slovakia
[b] National Physical Laboratory, Hampton Rd, Teddington, Middlesex TW11 0LW, UK

HIGHLIGHTS

- "Guest" molecules in "host" layered material were investigated.
- Amines and amino-acids were selected as guest molecules.
- Natural and synthetic host with smectite phyllosilicate structure were used.
- Dielectric properties were investigated by terahertz time domain spectroscopy.
- Resonance absorption peaks of guest were detected in far infrared region.

GRAPHICAL ABSTRACT

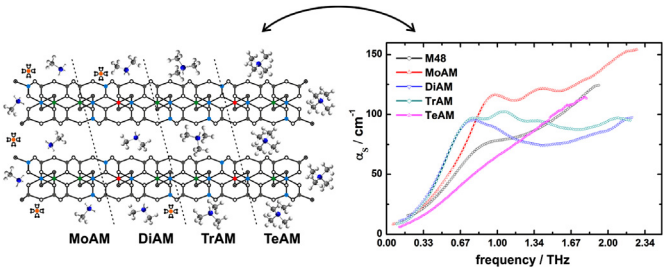

ARTICLE INFO

Article history:
Received 2 December 2013
Received in revised form
23 January 2014
Accepted 4 February 2014

This paper is dedicated to the Prof. Dr. Dr. h.c. Gerhard Lagaly at the occasion of his 75th birthday.

Keywords:
Inorganic compounds
Infrared spectroscopy (IR)
Powder diffraction
Dielectric properties
Optical properties

ABSTRACT

Layered clay minerals from the smectite group with different chemical composition and resulting layer charge (e.g. pyrophyllite, illite, hectorite and montmorillonite) were characterised for their dielectric properties in the far-infrared region using terahertz-time domain spectroscopy (THz-TDS). Samples with distinct cation exchange capacity such as hectorite and montmorillonite were modified using cation exchange reaction with alkylamines or amino acids. The presence of these species in 2D gallery was proved by X-ray diffraction and Fourier transform infrared spectroscopy. The frequency-dependent refractive index of these minerals was determined in the experimentally accessible range of 0.1–3.0 THz (3–100 cm^{-1}) using THz-TDS. Pristine samples revealed their refractive indices to be 1.82–2.15 at about 1 THz while the modified montmorillonite samples had their refractive indices changed by organic molecules used for their modification to 1.70–2.35 for amines and 1.97–2.36 for amino acids. The presence of organic substances in 2D gallery of clays was detectable despite the relatively high absorption of smectites with magnitude of 100 cm^{-1}.

1. Introduction

Layered clay minerals from the smectite group belong to the 2:1 clays where the basic structural layers are composed of two dimensional (2D) tetrahedral sheets formed by tetrahedrons [SiO_4] and one octahedral sheet typically formed from octahedrons [$Al(O,OH)_6$]. In a single smectite layer one octahedral sheet is sandwiched between two tetrahedral sheets terminated with hexagonally arranged oxygen atoms forming siloxane surface (Fig. 1) [1]. These oxygen atoms are involved in interactions with the neighbouring environment, and stacking of single smectite layers results in the formation of parent mineral particles. Generally, the chemical composition of smectites per unit cell contains two formula units which can be expressed as:

* Corresponding author. Tel.: +421 2 60296418; fax: +421 2 60296231.
E-mail addresses: marian.janek@fns.uniba.sk (M. Janek), mira.naftaly@npl.co.uk (M. Naftaly).

http://dx.doi.org/10.1016/j.matchemphys.2014.02.004
0254-0584/

$$M^{y+}_{\frac{(x+y)}{y}} \cdot (H_2O)_n \left\{ [Si_{4-y}Al_y] \left[M^{3+}, M^{2+}, M^{+} \right]^{(6-x)+}_{(2\approx 3)} O_{10}(OH)_2 \right\}^{(x+y)-}$$

Here the excess layer charge $(x + y)$- depends on the extent of isomorphous (charge non-equivalent) substitutions occurring in the tetrahedral (y) or octahedral (x) sheets. The excess charge localised in the layers is compensated by the hydrated exchangeable cations M^{y+} located between the layers and is responsible for the cation exchange capacity (CEC). This is connected to the layer charge via the molecular mass of the silicate framework unit (M_w/g mol^{-1}) by a simple relation: CEC $= (x + y)/M_w$ [2]. The cation exchange reaction represents one of the basic routes for easy and effective modification of the single particle interface, and thus the physical–chemical properties of pristine mineral. To follow systematic changes in the interlayer space of smectites, a simple characterisation tool is required by the chemist or physicist dealing with clay minerals.

Recent developments in terahertz-time domain spectroscopy (THz-TDS) operating in the far-infrared region may overcome the problems associated with employing conventional FTIR spectrometers for this type of investigation [3,4]. THz-TDS applications can be found in areas such as pharmaceuticals, biomolecular systems, dielectric materials or material quality control [5–7], but there is only a small number of papers dedicated to the inspection of layered or confined systems including clay minerals. To date, the THz-TDS technique was applied by Nagai et al. [8] for the investigation of dielectric properties of clay based polyamide nanocomposite films in the far-infrared region, leading to an interpretation of molecular interaction and relaxation times of polymer functional groups with montmorillonite surface. Janek et al. [9,10] using THz-TDS found that this technique can be successfully applied for investigating the dielectric properties of selected micaceous clay minerals and differentiating their spectral response in the far-infrared region, and for detecting host–guest intercalates of kaolinite or halloysite. [11] Recently, Wilke et al. [12,13] investigated the optical constants of montmorillonite in the THz region and calculated these values using the effective medium theory.

The main objectives of this paper are to foster the application of THz-TDS for the investigation of layered or confined 2D systems such as clay based materials, and to gain a better understanding of the processes involved during their physical–chemical modification based on the specific spectral response in the far infrared region. This technique enables measurement with high signal sensitivity and time-resolved phase information, allowing rich spectroscopic and dielectric analysis. For this purpose we used the terahertz time-domain spectroscopy technique based on femtosecond-laser driven photoconductive emitter and electro-optic detector in the frequency range of about 0.2–3.0 THz [14]. The selection of clay mineral samples was done in accordance with the known available microcrystalline species with significant differences in their chemical composition, which could be tested in the transmission mode of THz-TDS measurements.

The present study used the following mineral samples: pyrophyllite, hectorite, montmorillonite and illite, having different chemical compositions and cation exchange capacities (Table 1). All selected samples have smectite structure, where 6 negative charges per half unit cell are neutralized by two tri-valent cations e.g. montmorillonite (called dioctahedral occupancy). In contrast, this charge can be neutralized by three di-valent cations in trioctahedral minerals e.g. hectorite (Fig. 1). Depending on isomorphous structural substitutions and chemical composition, distinct particle swelling ability in aqueous environment can be observed in e.g. hectorite and montmorillonite, but no such swelling can be seen in pyrophyllite and illite. Despite the fact that the latter two samples have no cation exchange ability, they differ significantly from each other because pyrophyllite has inherently negligible excess layer charge (see formula unit above and Table 1), while illite represents a micaceous clay mineral variety with layer charge neutralized by exchangeable cations which are entrapped between the collapsed single mineral layers. For swelling clays, exchangeable interlayer cations can be easily replaced via the reaction of cation exchange using inorganic and/or organic cations, thus enabling preparation of layered organic–inorganic hybrid materials. Fast and reliable characterisation of physical properties of both pristine and modified minerals is of great interest. This is because these natural low cost materials have broad industrial utilization as pollution adsorbents, catalysts or catalyst support, foundry plasticizers in cosmetics, or are being investigated for novel application areas such as biosensors, electronic and optical devices [15,16].

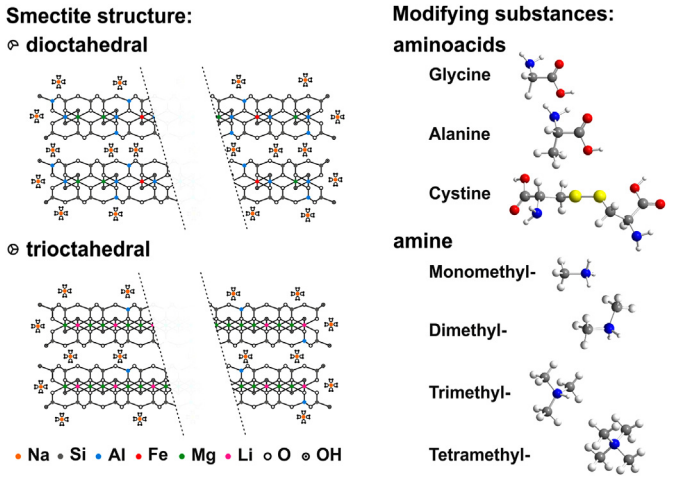

Fig. 1. Structure of dioctahedral 2:1 clay mineral; e.g. smectite layer showing isomorphous substitutions in tetrahedral and octahedral sheets with sodium as solvated exchangeable cations.

2. Experimental section

2.1. Materials

Idealised structural formulae of selected 2:1 clay minerals used in the present study are summarised in Table 1. As can be seen from this table, the clays differ in their cation density, CEC and ability to swell. Pyrophylite (PYR) and illite (ILL) were obtained from Wards

Table 1
Sample idealised structural formulae and determined cation exchange capacity.

Clay sample (origin)	Idealised structural formula	Cation Density charge/unit cell	CEC* mmol/g−1
Pyrophyllite≠ (North Carolina)	$\{[Si_4][Al_2]O_{10}(OH)_2\}$	0.00	0.00
Hectorite= (synthetic hectorite)	$M^+_{0.3} \cdot \{[Si_4][Mg_{2.7}Li_{0.3}]O_{10}(OH,F)_2\}$	0.30	0.72
Montmorillonite= (Wyoming)	$M^+_{0.4} \cdot \{[Si_{3.9}Al_{0.1}][Al_{1.5}Fe_{0.2}Mg_{0.3}]O_{10}(OH)_2\}$	0.40	0.89
Illite≠ (Illinois)	$M^+_{0.9} \cdot \{[Si_{3.2}Al_{0.8}][Al_{1.7}Fe_{0.2}Mg_{0.1}]O_{10}(OH)_2\}$	0.90	0.00

≠non-swelling; =swelling; *cation exchange capacity experimentally determined with copper triethylenetetramine complex [46].

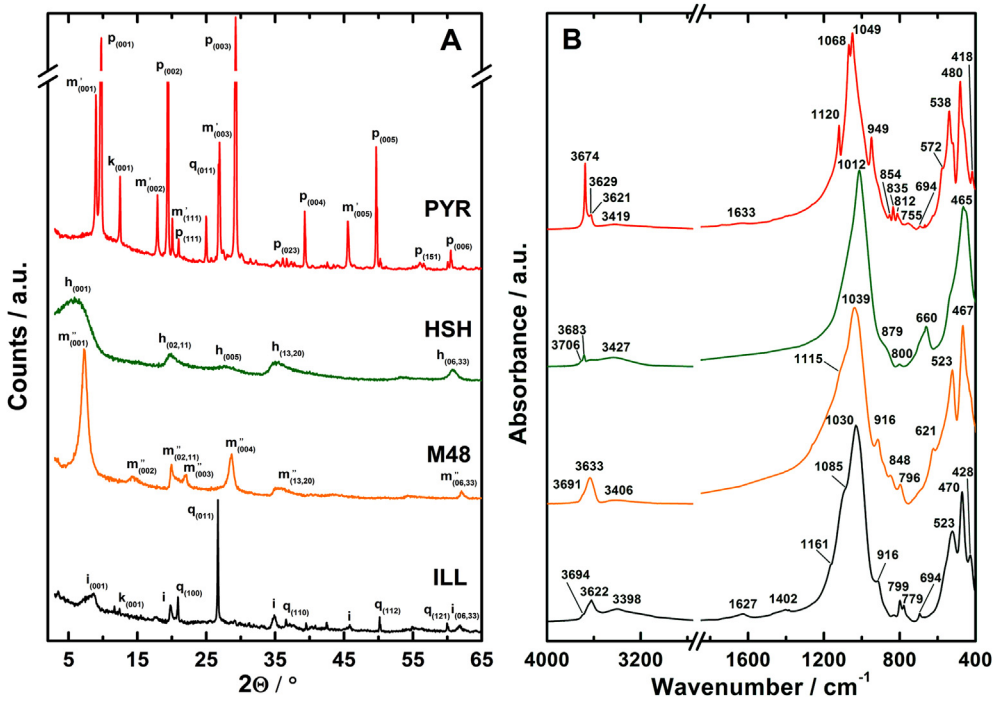

Fig. 2. A: X-ray powder diffraction patterns of used parent samples (PYR) pyrophyllite – p, (HSH) hectorite – h, (M48) montmorillonite – m″, (ILL) illite – i and admixtures of mica – m′, kaolinite – k and quartz – q with hkl indices. B: Corresponding FTIR spectra of respective minerals.

natural science establishment clay minerals repository and were used as received. The hectorite (HSH) and montmorillonite (M48) were received from the former Süd Chemie AG (currently Clariant International Ltd. Germany). No purification was needed for hectorite as synthetic sample; however, montmorillonite was washed using a standardized procedure to remove carbonates, iron oxides, humic materials, and fractionated to obtain the smaller-than-2-μm particles fraction according to Tributh and Lagaly [17,18]. A small amount of each sample was crushed in an agate mortar and used for X-ray diffraction on powder (XRPD) and for Fourier transform infrared (FTIR) analyses shown in Fig. 2A, B respectively.

Chemical modification of the interlayer space of swellable clays such as hectorite and montmorillonite was done using 25 mL dispersion with 2% solid content. Two different types of small organic molecules such as amines and amino acids were used for their surface modification. The first series used protonised amines: monomethylamine hydrochloride (MoA), dimethylamine hydrochloride (DiA), trimethylamine hydrochloride (TrA) and tetramethylammonium chloride (TeA), obtained from Aldrich. The second series used L-amino acids such as glycine (Gly) and L-alanine (Ala), from Lachema Brno, Czech Republic, and L-cystine (Cys) from Loba Chemie, Austria. Clay samples (0.5 g) were dispersed in a solution of respective chemical species with concentration of 33 mmol L^{-1} using an ultrasonic bath and horizontal shaker. The process of cation exchange is illustrated by Fig. 3, showing also the expression for the equilibrium constant. Here A^+ represent the original cationic species (e.g. Na^+ for montmorillonite) and B^+ are the protonated or cationic amines used for sample modification (Fig. 1).

Upon the ion exchange, the solid was separated from the supernatant by centrifugation at 6000 rpm, treated one more time with respective chemical solution in the ultrasonic bath and horizontal shaker, washed with demineralised water until the silver nitrate test for chloride anions was negative, air dried at 60 °C, and crushed in an agate mortar to be stored in Eppendorf PE ampoules. Each prepared sample was further used for XRPD and FTIR analyses. Both techniques confirmed the presence of organic molecules in the interlayer space and a successful exchange reaction of relevant mineral. For THz-TDS measurements, pellets of each sample were prepared by the pressed disk technique using at least 100 mg of sample material. The pellets used for THz-TDS experiments were approximately 1 mm thick and were prepared by applying manual force on torque with length of about 30 cm for 20 s. After THz-TDS measurements the porosity of randomly selected pellets was determined with helium picnometry, which revealed the mean around 43.0 ± 3.0%. For practical purpose the THz-TDS data represent values achieved from pellets measurements without

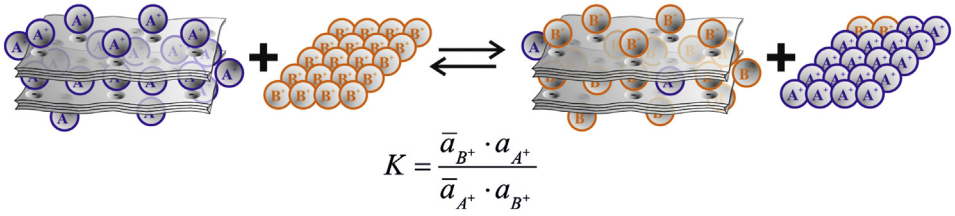

$$K = \frac{\bar{a}_{B^+} \cdot a_{A^+}}{\bar{a}_{A^+} \cdot a_{B^+}}$$

Fig. 3. Illustration of equilibrium reaction of cationic species A^+ with species B^+ bounded to the surface of clay layer and expression of equilibrium constant using activities of surface bounded ($\bar{a}$) vs. solvent present (a) species.

known porosity correction. Hence they represent the values which can be found for naturally accessible samples.

2.2. Techniques

X-ray diffraction patterns from all sample powders were obtained using PANalytical EMPYREAN X-ray powder diffractometer and Cu radiation (CuKα_1 λ = 0.154056 nm and CuKα_2 λ = 0.154439 nm with intensity ratio 2:1). The patterns were scanned in the range of 2.5–65° 2θ for parent materials and up to 25° 2θ in case of intercalates, with a step size of 0.039° and a counting time of 150.0 s/step.

FTIR spectrometer Nicolet Magna 750 equipped with a DTGS detector was used for infrared spectra measurements of powdered materials by the KBr pressed disc technique. The solid was homogenised using an agate mortar with spectroscopy grade KBr in a ratio of 1:200 mg. Spectra were recorded over the range of 4000–400 cm^{-1}, accumulating at least 64 spectral scans, with the spectral resolution of 4 cm^{-1}. The background signal was collected prior to every sample measurement. Spectra of all investigated samples in KBr disks were first measured after 24 h drying at 60 °C; then the parent samples were further dried at 80 °C during a period of 7 days and the FTIR spectra were collected again. The spectra were evaluated using the data collection and control software Omnic® (Thermo Electron Corporation).

The THz-TDS measurements were done on laboratory build equipment with standard configuration based on femtosecond-laser driven photoconductive emitter and electro-optic detection, the details of which can be seen elsewhere [19–24]. The THz-TDS has a bandwidth of approximately 4 THz with a peak signal-to-noise ratio of better than 40 dB [20]. All measurements were performed at the ambient temperature of 20.0 ± 1.0 °C, and the THz beam path was flushed with dry air to eliminate water absorption lines. The measurements were performed in transmission mode, with the pellet of clay sample mounted normal to the THz beam. The values of the frequency dependent complex refractive index were calculated from the transmission data as $\tilde{n}_S = n_S - i\kappa_S$, where n_S is the real refractive index and κ_S is absorption. The power absorption coefficient α_S of the samples was calculated from $\alpha_S = 2\kappa_S\omega/c$; where ω is the angular frequency and c the velocity of light in vacuum [25]. The power absorption coefficient is directly proportional to the optical density (absorbance) of the sample [26], hence is directly comparable to the spectral data obtained by other spectroscopic techniques.

3. Results and discussion

3.1. Material characteristics

X-ray diffraction patterns of the parent samples showing differences in the position of the first basal and other reflections are shown in Fig. 2A. These data confirm that hectorite (d = 1.40, 0.449, 0.256, 0.152 nm) and montmorillonite (d = 1.216, 0.618, 0.444, 0.404, 0.312, 0.254, 0.149 nm) samples represented pure mineralogical species of the studied layered type mineral. However, pyrophylite (d = 0.920, 0.460, 0.426, 0.306, 0.257, 0.241, 0.230, 0.184 nm) contained an admixture of mica (d = 0.992, 0.497, 0.443, 0.332, 0.256, 0.200 nm), kaolinite (d = 0.713, 0.443, 0.355, 0.256, 0.249 nm) and quartz (d = 0.425, 0.334, 0.246, 0.228, 0.213, 0.182, 0.154 nm), while illite (d = 1.02, 0.503, 0.448, 0.257, 0.198, 0.150 nm) contained quartz and kaolinite as an admixture. FTIR spectroscopy (Fig. 2B) confirmed the presence of quartz in the illite sample by showing the typical Si–O deformation bands at 799, 779 cm^{-1}, mica at 755, 694 cm^{-1} and a typical kaolinite stretching band as a shoulder at 3694 cm^{-1}. The pyrophyllite sample contained mica absorption bands at 3629, 755 and 694 cm^{-1}, and kaolinite was identified with the low intensity band at 3621 cm^{-1} [3,27–29]. The FTIR spectra of materials used in the present study, together with their bands attributions, can be found in papers

Table 2
a) Assignments of IR absorption bands of used layered clay minerals. b) Assignments of IR absorption bands of amines and amino acids.

Wavenumber (cm^{-1})	Attribution
a	
3545–3340	OH stretching vibrations of water
3360–3180	Overtone of OH deformation
1690–1600	OH deformation vibrations of water
Pyrophyllite	
3674	OH stretching of pyrophyllite structural hydroxyl groups
3629	OH stretching of mica structural hydroxyl groups
3621	OH stretching of kaolinite structural hydroxyl groups
1120	Si–O stretching (longitudinal mode)
1068	In-plane Si–O stretching
1049	In-plane Si–O stretching
949	OH deformation of inner hydroxyl groups
854–812	Si–O
755	Al–O–Al of MICA
694	Si–O of kaolinite
572	Si–O–Si deformation
538	Al–O–Si deformation
480	Si–O–Si deformation
418	Si–O
Hectorite	
3620	OH stretching of hectorite structural hydroxyl groups
1180	Amorphous silica and/or broken edges like, Si–O stretching
1079	Si–O stretching
1014	Si–O stretching
798	Si–O of silica and/or broken edges
656	Mg_3OH deformation
526	Si–O–Al (octahedral Al)
462	Si–O–Si bending
Montmorillonite	
3631	OH stretching of montmorillonite structural hydroxyl groups
1107	Si–O stretching (longitudinal mode)
1035	Si–O stretching
916	AlAlOH deformation
848	AlMgOH deformation
794	Si–O of silica and/or broken edges
623	Coupled Al–O and Si–O, out-of-plane
523	Al–O–Si deformation
464	Si–O–Si deformation
Illite	
3694	OH stretching of kaolinite structural hydroxyl groups
3622	OH stretching of illite structural hydroxyl groups
1402	CO_3 stretching of calcite
1161	Si–O stretching of quartz
1085	Perpendicular Si–O stretching
1030	Si–O stretching
916	AlAlOH deformation
799	Si–O stretching of quartz
779	Si–O stretching of quartz
694	Si–O stretching of quartz
523	Al–O–Si deformation
470	Si–O–Si deformation
428	Si–O deformation
b	
3400–3300	NH stretching
3300–2500	OH stretching of carboxylic acids
2965–2750	CH, CH_2, CH_3 stretching
2600	NH^+ stretching
1725–1695	C=O stretching of carboxylic acid
1650–1590	NH deformation
1250	COH stretching or CH_2 deformation
1460–1360	CH_2, CH_3 deformation
1160–1060	C–N stretching
950–910	OH deformation of carboxylic acids
850	NH deformation
800–600	NH, NH_2 wag in amines

dedicated to various studies using several investigation techniques [3]. Briefly, in the mid infrared region 2:1 layered silicates have the typical absorption bands of structural OH groups. The OH stretching bands are identified in the region of 3630–3610 cm^{-1}; whereas deformation bands reflecting the chemical composition of the layers, e.g. AlAlOH, AlFeOH and AlMgOH, can be found at 917–913 cm^{-1}, 887–884 cm^{-1}, 846–837 cm^{-1}, respectively. A typical feature is the presence of intense SiO stretching bands at 1120–990 cm^{-1} and deformation bands of bonds such as Al–O–Si and Si–O–Si. Where the material has adsorbed water molecules, these can be found as stretching and deformation vibrations at 3545–3340 and 1690–1600 cm^{-1}, respectively. A more detailed assignment of IR absorption bands is summarised in Table 2a.

Due to the fact that only Montmorillonite and Hectorite could be chemically modified by the cation exchange reaction using suitable molecules (Table 1), the modification of the interlayer space of these minerals was performed using selected model substances of amines and amino acids having low molecular weight. These were selected in order to test the possibility of direct identification of specific molecular or functional groups when presented in the confined environment of interlayer space. Smaller molecular species are expected to be more suitable for theoretical calculations of corresponding vibration bands in the far-infrared region, e.g. using Density Functional Theory, Hartree–Fock approximations or molecular dynamics simulations [30–33]. There have been a number of studies published on the THz spectroscopy of pure amino acids [34,35], their dimers [36] and sulphur containing amino acids [37,38]. However, to our knowledge there are no FIR data available for these substances contained in confined layered environment.

The results of X-ray diffraction of the parent material and its varieties modified with selected substances are shown in Fig. 4A for M48 and in Fig. 4B for HSH. XRPD patterns of Montmorillonite show a distinct change in the position of its first basal (d_{001}) reflection, while a simultaneous change of the peak shape can also be observed depending on the modification molecule being used. Changes in the first basal peak position are in the range of a few tenths nm, because the sizes of intercalated molecules are comparable to the original hydrated Na^{+} cations occupying the interlayer space. Observed changes correspond to a change of the gallery height in the range of about 0.02–0.17 nm, e.g. in the case of Cys or TeA molecules the basal distance on the level of 1.33 and 1.38 nm, respectively. This basal distance at the level of 1.37 nm corresponds approximately to the thickness of smectite's primary amines intercalates with the alkyl chain having about 6 carbon atoms. The changes in the position of the first basal reflection of *n*-alkylamine series have been used for the determination of the mean layer charge and the layer charge density distribution [2].

In the case of Hectorite sample, XRPD shows a much broader peak of its first basal reflection (d_{001}) than Montmorillonite (Fig. 4A, B). This is due to the much lesser lateral size of HSH particles [39]. For instance, this sample is able to form transparent aqueous dispersions or gels at concentrations of >2 mass%, while turbid dispersions are formed with M48, indicating that particle size of HSH is below the wavelength size of visible light (<380 nm) [40]. Nevertheless, the change in the peak shape and position of the first basal reflection was clearly detected for all modified samples. To confirm further the successful modification of interlayer gallery of studied clays with selected molecules by an independent method, they were characterised by FTIR in the mid-IR. The spectra of modified smectites (solid lines) along with the spectra of pure modifying substances (dotted lines) are shown in Figs. 5 and 6. Assignments of typical IR absorption bands of modifying amines and amino acids are summarised in Table 2b.

FTIR spectra of modified Montmorillonite (Fig. 5) show the following. i) In the interlayer space there are present hydrated organic cations, because the water OH stretching band at 3425–3435 cm^{-1} and an overtone of the deformation band at 3232–3270 cm^{-1} are observed in the 3900–2700 cm^{-1} region. ii) The confinement of molecules in the interlayer space changes significantly their absorption bands in the 1950–1350 cm^{-1} region, although some bands retain their original positions e.g. in DiA, TrA, TeA. iii) Only minor changes of stretching Si–O vibrations are resolvable in the 1050–450 cm^{-1} region, such as enhancement or weakening of the shoulder at the 1115 cm^{-1}, but these are

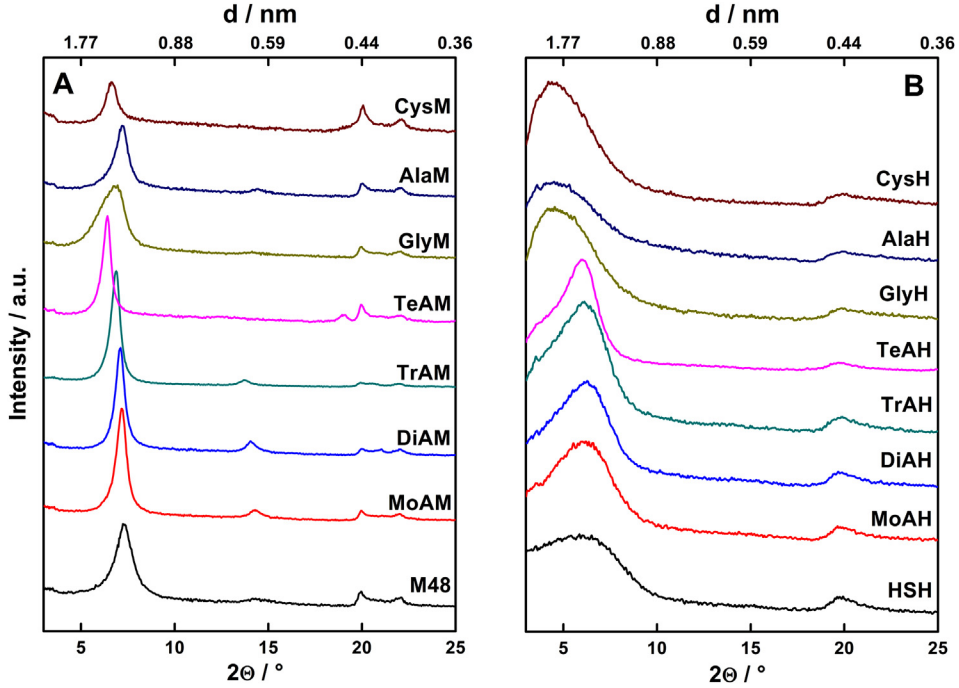

Fig. 4. Changes in the positions of the first basal reflection of montmorillonite intercalates – A – and Hectorite – B – modified with (M48/HSH) – parent material, (MoA) – methylamine, (DiA) – dimethylamine, (TrA) – trimethylamine, (TeA) – tetramethylamine, (Gly) – glycine, (Ala) – alanine, (Cys) – cystine.

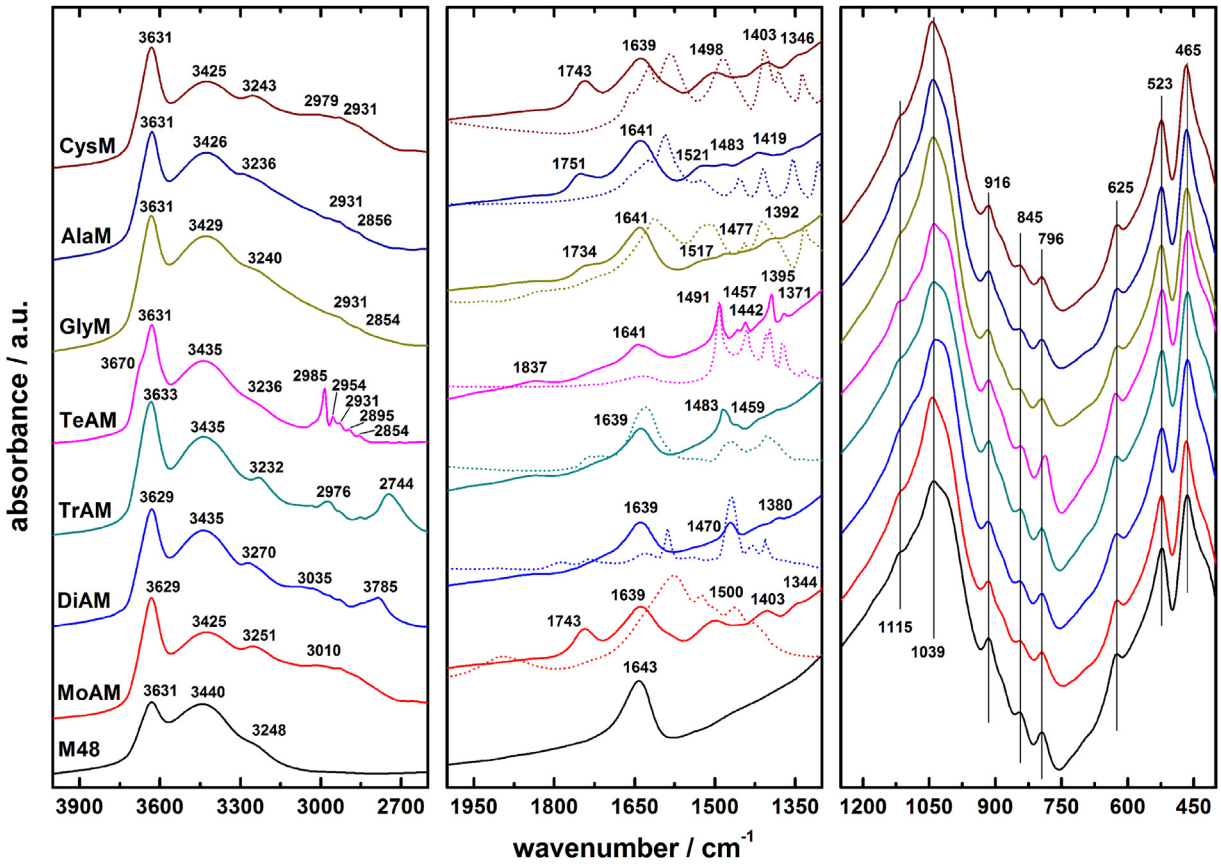

Fig. 5. FTIR spectra of Montmorillonite intercalate modified with (M48) – parent material, (MoA) – methylamine, (DiA) – dimethylamine, (TrA) – trimethylamine, (TeA) – tetramethylamine, (Gly) – glycine, (Ala) – alanine, (Cys) – cystine.

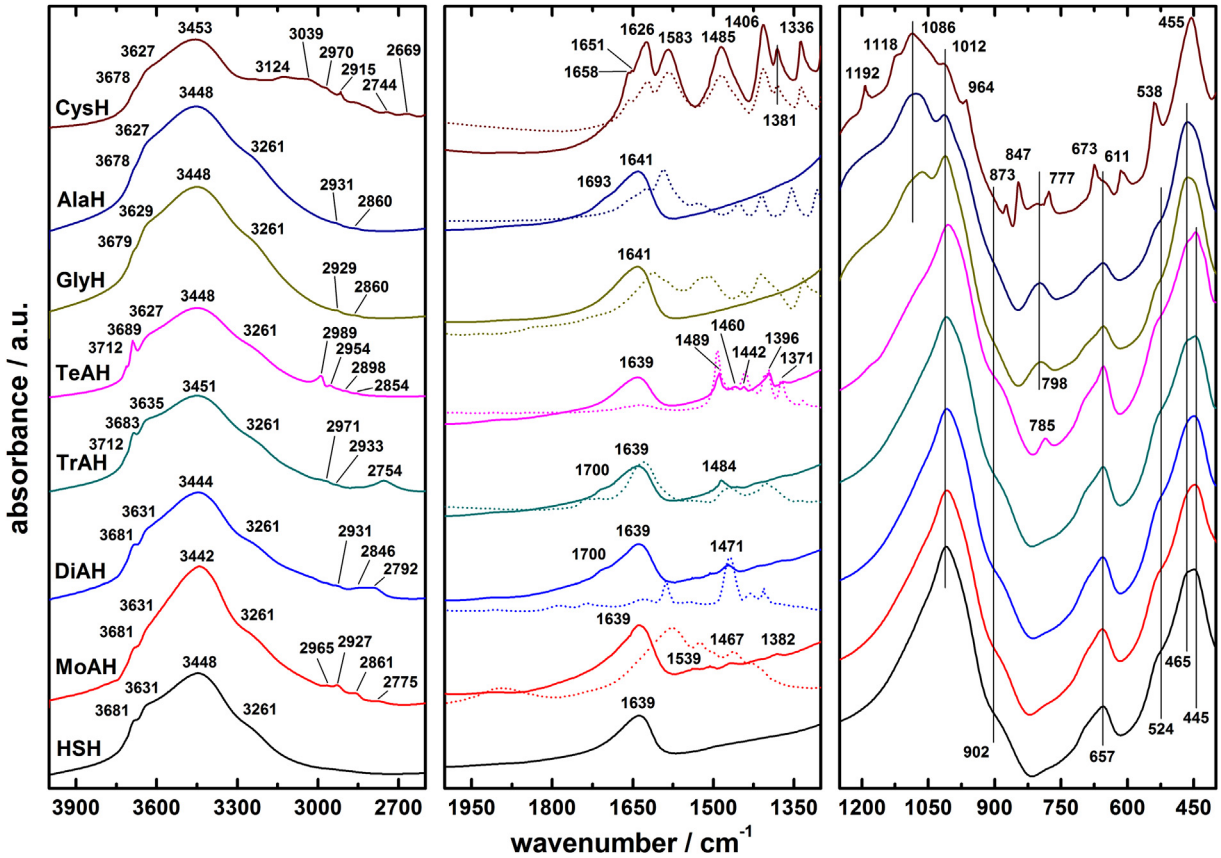

Fig. 6. FTIR spectra of hectorite intercalate modified with (HSH) – parent material, (MoA) – methylamine, (DiA) – dimethylamine, (TrA) – trimethylamine, (TeA) – tetramethylamine, (Gly) – glycine, (Ala) – alanine, (Cys) – cystine.

insignificant changes in comparison with deformation vibrations in the parent M48 spectrum of e.g. OH, Al–O–Si, or Si–O–Si.

For modified samples of Hectorite (Fig. 6) the FTIR spectral features indicated the following. i) The modification of this sample with amines influences the OH stretching vibrations, resulting in the gradual appearance of a well resolved shoulder and/or band in samples modified with MoA, DiA, TrA and TeA, converging to 3712 and 3689 cm^{-1}. The water OH stretching band at 3442–3453 cm^{-1} and the overtone of deformation band as shoulder at 3261 cm^{-1} are observed in the 3900–2700 cm^{-1} region. ii) Because of the smaller particle lateral diameter and smaller cation exchange capacity value of hectorite, the number of molecules confined in the interlayer space is lower than in the case of montmorillonite. But, under such conditions, a higher fraction of molecules could be located at the particle edges. However, bands of lesser intensities than in the case of montmorillonite are observed in the 1950–1350 cm^{-1} region, corresponding to modification molecules, except for Cystine modified hectorite. iii) In contrast to montmorillonite, more changes of stretching Si–O vibrations were observed, such as the appearance of a band at the 1086 cm^{-1} for CysH, AlaH, and GlyH. The presence of these compounds in the interlayer space can be seen in the appearance of vibrations at 798 cm^{-1} and 785 cm^{-1} found in TeAH. It was interesting to observe intense absorption bands of Cystine in each spectral region of modified hectorite. This indicated a relatively high affinity of this molecule for the hectorite surface in comparison with other amino-acids used. Such intensive interaction may be a consequence of the synergetic effect of e.g. Cystine functional groups, with suitably configured hectorite OH edge groups involved in the chemical interaction. The formation of effective H-bonds was found to be essential for the peptide bonds formation catalysed by clay surfaces [41–43].

The results observed by XRPD and FTIR proved that organic–inorganic hybrid materials were successfully prepared with confined molecules present in the interlayer space of Montmorillonite, where these molecules interact with its siloxane surface. In the case of Hectorite the modifying molecules are present also in the interlayer space, but they may interact intensively with a large fraction of OH groups localised at the edges of the particles. These differences are clearly connected to the morphological differences among selected swelling smectites.

3.2. Optical characteristics in THz region

The mineralogical variability of the selected clay minerals with their different chemical compositions (Table 1) offered a unique opportunity to compare their dielectric and spectral properties in far-IR region. The frequency dependence of the refractive index n_S and absorption coefficient α_S of parent clays in the range of 0.1–3.0 THz (3–100 cm^{-1}) as determined by THz-TDS is shown in Fig. 7A. The refractive indices of PYR, HSH, M48 and ILL found in these types of minerals at e.g. 1 THz had the following values: 2.10 – PYR, 1.82 – HSH, 2.15 – M48, 2.15 – ILL. These refractive indices are lower than those observed in micas with various chemical compositions (2.39–2.78@1 THz) [9,10]. The dispersion of refractive index n_S in studied frequency windows (Fig. 7A) was much lower for PYR and ILL ($\sim$0.05), than for HSH and M48 samples ($\sim$0.17).

Very interesting results of different frequency dependence of absorption coefficient α_S, in the studied samples can be seen in Fig. 7B. The steepest rise of absorption coefficient with frequency is seen in HSH and M48, while the weakest is shown by PYR. This behaviour can be due either to the water content present as physically adsorbed molecules on the particle surface of PYR and ILL, or as hydration water of exchangeable cations in HSH and M48 samples. The differences in the chemical composition of selected samples and their crystallographic structure may also be responsible for the observed behaviour. The absorptive properties of all samples in the far-infrared region are relatively high and reach the values of tens cm^{-1} (e.g. 15–78@1 THz). However, only M48 and PYR showed absorption bands at around 0.89 THz (29.7 cm^{-1}) and 2.28 THz (76.1 cm^{-1}), respectively. Different positions of low frequency bands in the region of 50–200 cm^{-1} were found by Laperche and Prost [44] in micas containing various inorganic exchangeable cations such as K^+, Rb^+, Cs^+, NH_4^+ and Ba^{2+}. The bands observed in M48 and PYR can therefore be associated with low frequency skeletal vibrations of the smectite structure, or in the case of M48, with low frequency vibration of exchangeable cations of this mineral. However, as was shown by Laperche and Prost [4], the final position of the low frequency bands is affected by both the type of layered clay mineral and the type of exchangeable cation represented, e.g. by its characteristic molecular mass.

The frequency dependence of refractive indices and absorption coefficients of amine modified montmorillonite and hectorite are shown in Fig. 8. A distinct effect of amines can be seen on the spectral response of modified M48 as the number of CH_3 groups changes from 1 to 4 in the mono-, di-, tri- and tetra-methylamine. The refractive indices of M48 and its amine forms were found to be in the range of 1.70–2.35, while pristine M48 exhibited the highest value of refractive index. In addition, clear absorption bands can be observed, which change their position and shape with amine treatment. The low frequency band observed at 0.89 THz (29.7 cm^{-1}) in pristine M48 changed its position after modification

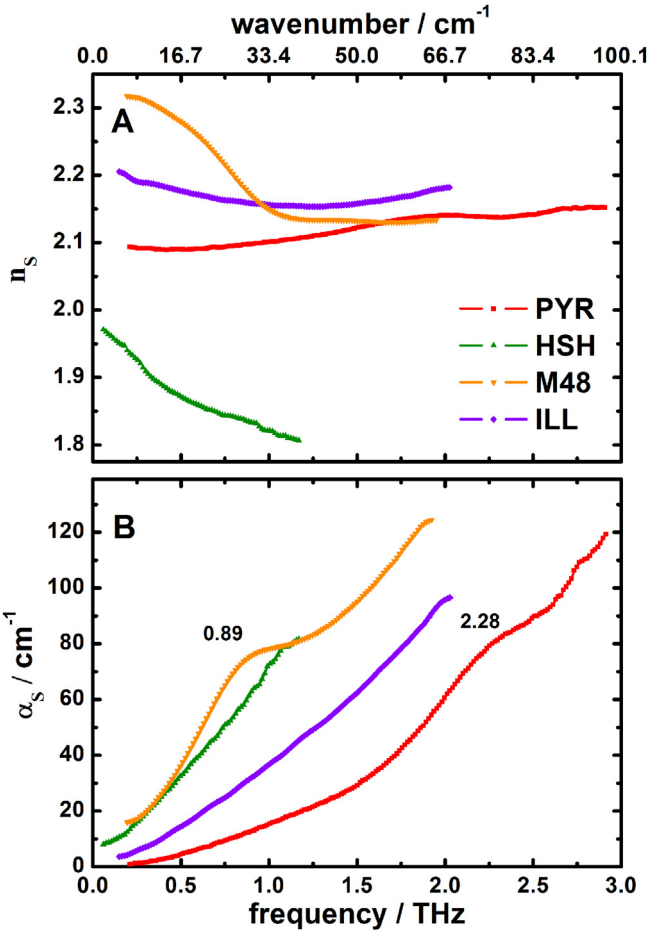

Fig. 7. Frequency dependence of refractive index – n_S and power absorption coefficient – α_S of pyrophyllite (PYR), hectorite (HSH), montmorillonite (M48), and illite (ILL).

of M48 with mono-methylamine, while two distinct bands at 0.96 and 1.39 THz (32.0 and 46.4 cm^{-1}) appeared in MoAM. A typical spectral response can be found for each of the amines used: hence, di-methylamine (DiAM) revealed one broad band at 0.78 THz (26.0 cm^{-1}), tri-methylamine (TrAM) showed three bands starting at the lowest frequency of 0.75 THz (25.0 cm^{-1}), overlapping with 1.06 and 1.38 THz (35.3 and 45.9 cm^{-1}), and finally tetra-methylamine (TeAM) had no bands in the studied THz region. These observations confirm the potential of THz-TDS as a suitable technique for the investigation of layered confined systems such as clay based hybrid materials, despite the relatively high far infrared absorption of clays of the order of 100 cm^{-1}.

Indeed, the effect of clay mineral used is clearly seen in a similar hectorite sample set (Fig. 8). The mono-, di- tri- and tetra-methylamine modified HSH shows no detectable spectral bands in the frequency window of 0.05–2.50 THz. The reason why these amines were not resolved in the hectorite sample must be connected to the concentration of organic species present in the HSH sample. This difference is also seen in the mid-IR, where HSH samples modified with amines showed greatly reduced intensities of absorption bands (Figs. 5 and 6).

An important factor affecting the ability of swelling clays to adsorb cationic organic molecules is the cation exchange capacity of the respective clay mineral. As seen in Table 1, HSH has about 20% less cation exchange capacity than M48, but this fact only seems insufficient to explain the observed differences. In this case also the morphology of particles and the location of exchangeable positions should play an important role. As mentioned above, the HSH particles used in the study had much smaller lateral dimensions than M48 particles, and as such had a much higher contribution of the particle edge sites to the total cation exchange capacity [45]. The particle size difference can be expected to affect the affinity of used amines towards the exchangeable positions, while their location at the particle edges could either decrease or increase it. In this sample set, the tetramethylammonium cation apparently had sufficient affinity, as could be expected from mid-FTIR measurements and from the FWHM (full width at half maximum) of the first basal diffractions seen in the XRPD patterns of TeAM and TeAH (Figs. 4–6). Unfortunately, this substance was not observable in the investigated THz region even for TeAM.

A different situation was observed for M48 and HSH samples modified with Gly, Ala and Cys. As discussed above, GlyM, AlaM and CysM affected the mid-IR spectra, exhibiting significant spectral changes: however, in the case of hectorite, only the CysH sample revealed vibration bands with noticeable intensities, which were clearly higher than in the case of the CysM sample (Fig. 6). The frequency dependence of refractive indices and absorption coefficients of montmorillonite and hectorite modified by amino acids is shown in Fig. 9. A low frequency band in GlyM was observed at 0.94 THz (31.5 cm^{-1}). Very similar behaviour is seen in AlaM which has a band at 0.91 THz (30.5 cm^{-1}). CysM has a distinct band at 0.88 THz (29.3 cm^{-1}). The refractive indices of M48 modified by amino acids were in the range of 1.97–2.36, comparable to the amine modified M48 refraction values. In the case of HSH the refractive indices lie in a much narrower interval in the range of 1.60–1.74. While the GlyH and AlaH samples did not show any absorption bands, CysH revealed three distinct absorption bands at 0.72, 1.50 and 2.03 THz (24.0, 50.0 and 67.6 cm^{-1}). These

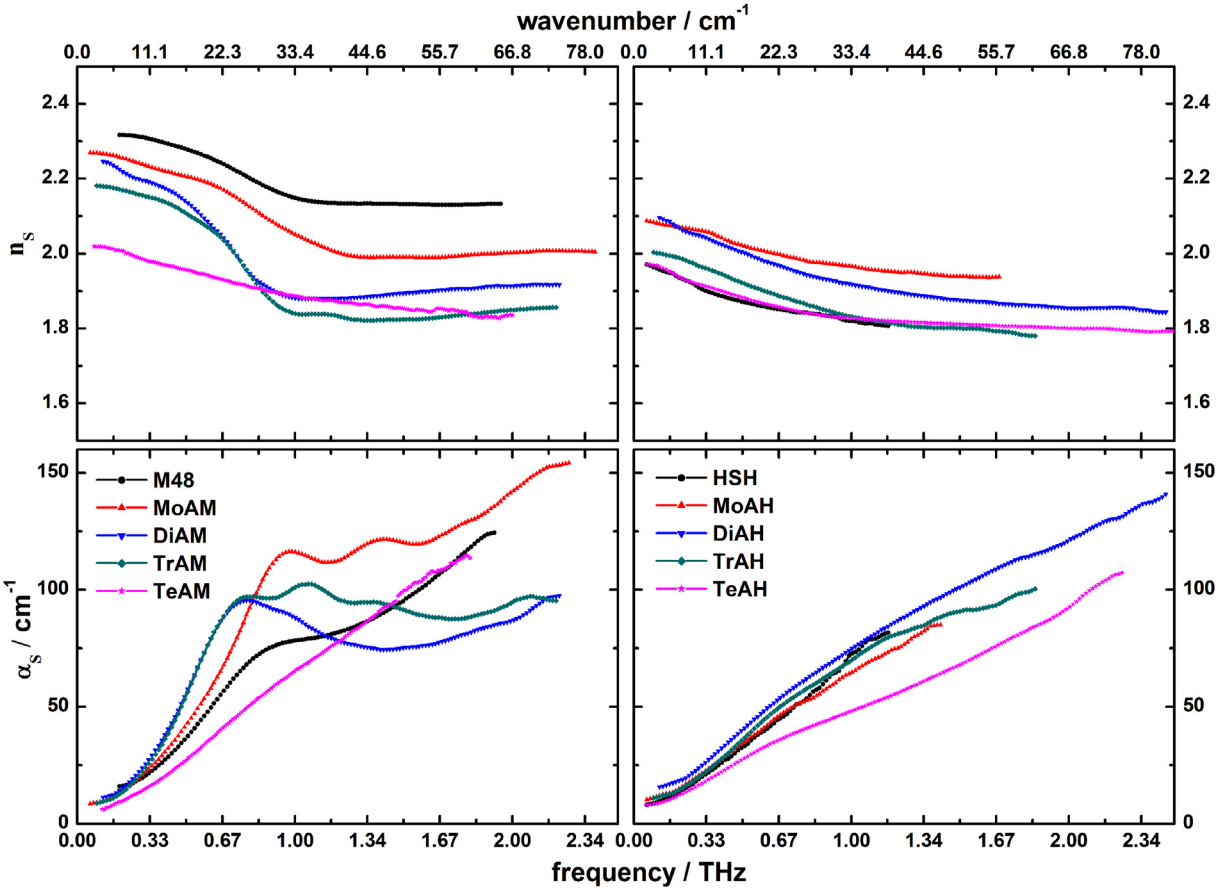

Fig. 8. Frequency dependence of refractive index – n_S and power absorption coefficient – α_S of HSH and M48 samples modified with amines: methylamine (MoA), dimethylamine (DiA), trimethylamine (TrA), tetramethylamine (TeA).

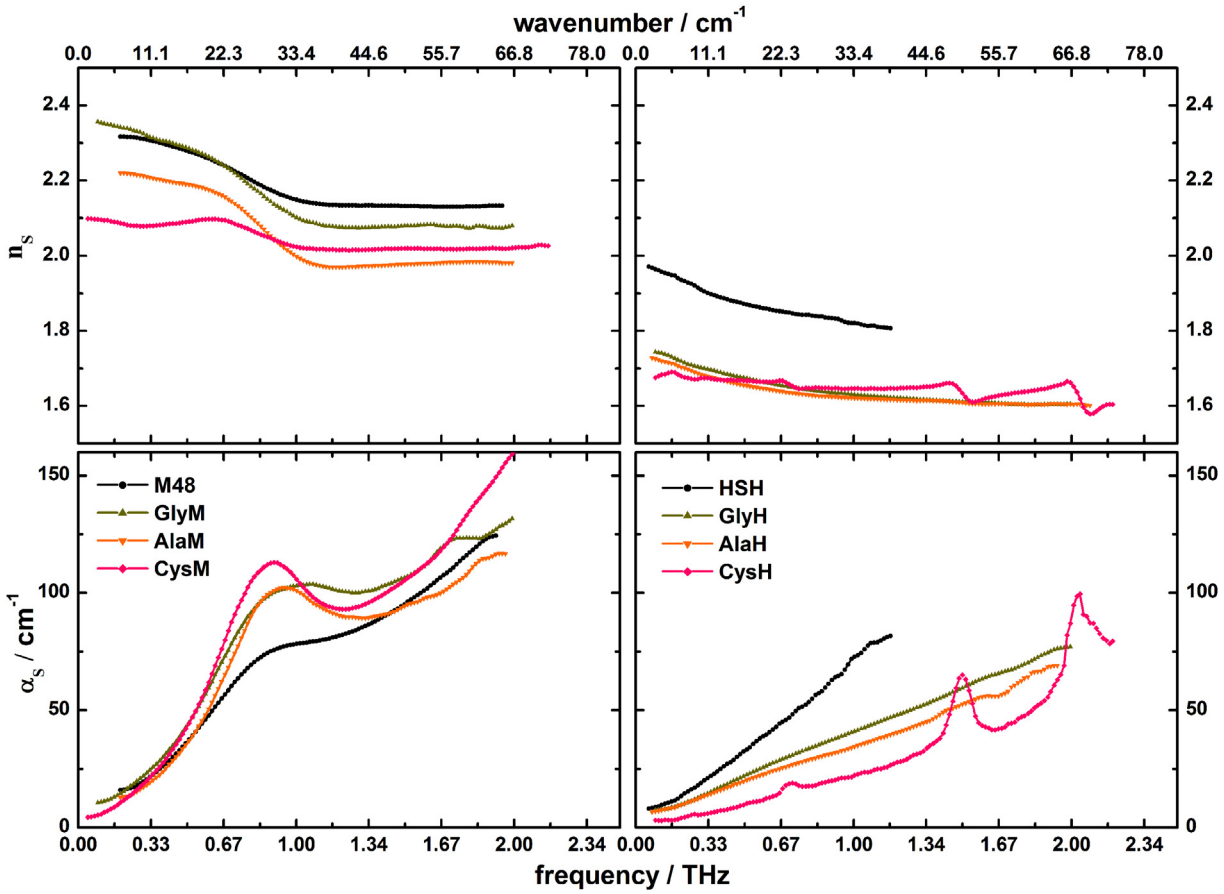

Fig. 9. Frequency dependence of refractive index – n_S and power absorption coefficient – α_S of HSH and M48 samples modified with amino acids: glycine (Gly), alanine (Ala), cystine (Cys).

bands appear close to the positions observed by Yamamoto et al. [37] and Brandt et al. [38] in investigating sulphur-containing peptide dimers by THz-TDS.

The results seen for M48 and HSH modified by amino acids demonstrate the difficulty of assigning the observed bands to the respective species present in the interlayer space of layered minerals. As mentioned above, the low frequency bands are affected by the type of layered clay mineral and the type of molecule introduced in the interlayer space. However, this would assume a 100% exchange of the original interlayer cations, which may often be an overestimate due to the different affinity of exchanged species towards clay surface in equilibrium reaction (Fig. 3). In cases where the low affinity of exchanged species towards clay surface results in low values of the equilibrium constants, only a small fraction of original exchangeable cations would be exchanged. Under such conditions, the position of the low frequency bands associated with the original exchangeable cations would not significantly change, as a significant fraction of them still remains in the interlayer space.

This is probably the case for M48 modified by amino acids, since relatively small amounts of glycine were expected to be adsorbed on various clays according to studies reported by Bujdák and Rhode [41–43] dedicated to catalytic performance of layered silicates in peptide bond formation. The high intensities of low frequency bands [37,38] found in cystine-modified hectorite sample must therefore be the consequence of the high affinity of this species towards the surface of HSH with a high equilibrium constant value. These results indicate that a study of a modified series with well-defined amounts of respective species can lead to an estimation of species occupancy in the interlayer space. For this reason there are significant opportunities in applying THz-TDS to the identification of such chemical substances and to their further characterisation when located in the confined environment represented by interlayer 2D galleries.

4. Conclusions

Presented study showed that microcrystalline clay minerals such as pyrophyllite, illite, hectorite and montmorillonite can be successfully investigated using terahertz-time domain spectroscopy in the far-infrared region. Frequency-dependent refractive indices and absorption coefficients of these minerals were measured using the pressed disc technique. Samples with distinct cation exchange capacity prior and after their modification with alkylamines or amino acids were also studied. THz-TDS proved its potential for the investigation of species, introduced in the 2D gallery of mineral interlayer, which have high affinity towards clay surface, are chemically bounded, or were prepared as fully saturated with species introduced. Such chemical substances can be identified by their low frequency vibration bands. This can be further used for the study of equilibrium processes or reactions of organic molecules in the 2D confined environment offered by layered silicates.

Acknowledgements

The assistance of Dr. A. Brtáňová (Institute of Inorganic Chemistry, Slovak Academy of Sciences) during XRPD measurements is greatly acknowledged. We wish to thank to Comenius University

for supporting of the PhD. work of D. Zich with the UK Grants No. 298/2012, 338/2011, 309/2010. The financial support of the Slovak Grant Agency for Science VEGA (grant No. 1/0943/13) and of the Slovak Research and Development Agency APVV (grant APVV-0291-11) is greatly appreciated. Work at NPL was supported by the National Measurement Office of the U.K.

References

[1] F. Bergaya, G. Lagaly (Eds.), Handbook of Clay Science, second ed., Elsevier Amsterdam, 2013.
[2] G. Lagaly, Layer charge determination by alkylammonium ions, in: A.R. Mermut (Ed.), Clay Minerals Society Workshop Lectures 6, Layer Charge Characteristics of 2:1 Silicate Clay Minerals, 1994, pp. 1–46. Boulder, Colorado.
[3] J. Madejová, P. Komadel, Clays Clay Min. 49 (2001) 410–429.
[4] R. Prost, V. Laperche, Clays Clay Min. 38 (1990) 351–355.
[5] X.-C. Zhang, J. Xu, Introduction to THz Wave Photonics, Springer, Heidlelberg, 2010.
[6] K.-E. Peiponen, J.A. Zeitler, M. Kuwata-Gonokami, Terahertz Spectroscopy and Imaging, Springer, Heidlelberg, 2013.
[7] D. Saeedkia, Handbook of Terahertz Technology for Imaging, Sensing and Communications, Woodhead Publishing, Oxford (, 2013.
[8] N. Nagai, T. Imai, R. Fukasawa, K. Kato, K. Yamaguchi, Appl. Phys. Lett. 85 (2004) 4010–4012.
[9] M. Janek, I. Bugár, D. Lorenc, V. Szöcs, D. Velič, D. Chorvát, Clays Clay Min. 57 (2009) 416–424.
[10] M. Janek, M. Matejdes, V. Szöcs, I. Bugár, A. Gaál, D. Velič, J. Darmo, Philos. Mag. 90 (2010) 2399–2413.
[11] D. Zich, T. Zacher, J. Darmo, V. Szöcs, D. Lorenc, M. Janek, Vib. Spectrosc. 69 (2013) 1–7.
[12] I. Wilke, V. Ramanathan, J. LaChance, M. Aldersley, P. Joshi, J. Ferris, in: The 38th International Conference on Infrared, Millimeter and Terahertz Waves, Mainz on the Rhine, Germany, 2013. Extended Abstract TU14–4.
[13] I. Wilke, V. Ramanathan, J. LaChance, A. Tamalonis, M. Aldersley, P.C. Joshi, J. Ferris, Appl. Clay Sci. 87 (2014) 61–65.
[14] S.L. Dexheimer, Terahertz Spectroscopy – Principles and Applications, CRC Press Taylor & Francis Group, Boca Raton Florida, USA, 2008.
[15] G. Schulz-Ekloff, D. Wöhrle, B. van Duffel, R.A. Schoonheydt, Microporous Mesoporous Mater. 51 (2002) 91–138.
[16] S. Takagi, T. Shimada, Y. Ishida, T. Fujimura, D. Masui, H. Tachibana, M. Eguchi, H. Inoue, Langmuir 29 (2013) 2108–2119.
[17] H. Tributh, G. Lagaly, GIT Fachz. Lab. 30 (1986) 524–529 (in German).
[18] H. Tributh, G. Lagaly, GIT Fachz. Lab. 30 (1986) 771–776 (in German).
[19] M. Naftaly, J. Leist, Appl. Opt. 52 (2013) B20–B25.
[20] J. Kröll, J. Darmo, K. Unterrainer, Electron. Lett. 40 (2004) 763–764.
[21] M. van Exter, Ch. Fattinger, D. Grischkowsky, Appl. Phys. Lett. 55 (1989) 337–340.
[22] K. Reimann, Rep. Prog. Phys. 70 (2007) 1597–1632.
[23] Q. Wu, X.-C. Zhang, IEEE J. Sel. Top. Quant. Electron. 2 (1996) 693–700.
[24] G. Zhao, R.N. Schouten, N. van der Valk, W.Th. Wenckebach, P.C.M. Planken, Rev. Sci. Instrum. 73 (2002) 1715–1720.
[25] W. Withayachumnankul, M. Gretel, Y. Xiaoxia, S. Atakaramians, I. Jones, H. Lin, B.S.Y. Ung, J. Balakrishnan, B.W.-H. Ng, B. Ferguson, S. Mickan, B.M. Fischer, D. Abbott, Proc. IEEE 95 (2007) 1528–1558.
[26] M. Fox, Optical Properties of Solids, Oxford University Press, New York, 2001, p. 305.
[27] V.C. Farmer, Spectrochim. Acta A 56 (2000) 927–930.
[28] J. Madejová, J. Kečkéš, H. Pálková, P. Komadel, Clay Miner. 37 (2002) 377–388.
[29] J. Madejová, Vib. Spectrosc. 31 (2003) 1–10.
[30] M. Takahashi, Y. Kawazoe, Y. Ishikawa, H. Ito, Chem. Phys. Lett. 429 (2006) 371–377.
[31] M. Takahashi, Y. Ishikawa, H. Ito, Chem. Phys. Lett. 531 (2012) 98–104.
[32] Q. Wang, H.L. Wang, Chem. Phys. Lett. 534 (2012) 72–76.
[33] S. Funkner, G. Niehues, D.A. Schmidt, M. Heyden, G. Schwaab, K.M. Callahan, D.J. Tobias, M. Havenith, J. Am. Chem. Soc. 134 (2012) 1030–1035.
[34] C.S. Ponseca Jr., O. Kambara, S. Kawaguchi, K. Yamamoto, K. Tominaga, J. Infrared Millimeter Terahertz Waves 31 (2010) 799–809.
[35] Z.-P. Zheng, W.-H. Fan, J. Biol. Phys. 38 (2012) 405–413.
[36] D.F. Plusquellic, K. Siegrist, E.J. Heilweil, O. Esenturk, Chem. Phys. Chem. 8 (2007) 2412–2431.
[37] K. Yamamoto, Md. H. Kabir, K. Tominaga, J. Opt. Soc. Am. B 22 (2005) 2417–2426.
[38] N.N. Brandt, A.Yu. Chikishev, A.V. Kargovsky, M.M. Nazarov, O.D. Parashchuk, D.A. Sapozhnikov, I.N. Smirnova, A.P. Shkurinov, N.V. Sumbatyan, Vib. Spectrosc. 47 (2008) 53–58.
[39] V.A. Drits, D.D. Eberl, J. Środo&nacute, Clays Clay Miner. 46 (1998) 38–50.
[40] M. Janek, G. Lagaly, Colloid Polym. Sci. 281 (2003) 293–301.
[41] J. Bujdák, B.M. Rode, J. Mol. Catal. A Chem. 144 (1999) 129–136.
[42] J. Bujdák, B.M. Rode, Silica Orig. Life Evol. Biosphere 29 (1999) 451–461.
[43] J. Bujdák, B.M. Rode, J. Pept. Sci. 10 (2004) 731–737.
[44] V. Laperche, R. Prost, Clays Clay Miner. 39 (1991) 281–289.
[45] M. Janek, P. Komadel, G. Lagaly, Clay Miner. 32 (1997) 623–632.
[46] L.P. Meier, G. Kahr, Clays Clay Miner. 47 (1999) 386–388.